DESIGN AN ADAPTIVE FINITE TIME CONTROLLER FOR INTEGRATED GUIDANCE CONTROL SYSTEMS BY USING FINITE DISTURBANCE OBSERVER AND BACKSTEPPING TECHNIQUE

Hong Toan Dinh[1,*], Dang Khoa Truong[1], Ngoc Anh Mai[2], Van Nguyen Pham[1], Quy Tran[1], Cong Dinh Nguyen[1]

[1]*Institute Control Engineering, Le Quy Don Technical University*

[2]*Advanced Technology Center, Le Quy Don Technical University*

Abstract

A novel control synthesis approach for integrated guidance and control (IGC) systems in aerial vehicle (AV), based on finite-time backstepping (FTB) combined with a finite-time disturbance observer (FTDO) is proposed. Comparing to the conventional backstepping methods ensuring asymptotic convergence, the proposed approach guarantees finite-time convergence and significantly improves disturbance rejection capability. The controller is designed in a strict-feedback structure containing layers employing nonlinear control laws to satisfy Lyapunov stability conditions. Individual FTDOs are constructed for each state equation to accurately estimate the lumped disturbances and enhance compensation performance. Simulation results show that the proposed method shortens transient response time, reduces control errors, and ensures accurate target tracking even under strong disturbance conditions.

Keywords: *Integrated guidance and control (IGC); finite-time backstepping (FTB); finite-time disturbance observer (FTDO); maneuvering target; lumped disturbance.*

1. Introduction

Modern aerial vehicle (AV) systems require high-precision interception capabilities against maneuvering targets under varying disturbances. In traditional control structures, the guidance loop and the autopilot loop are designed separately, leading to drawbacks such as time delays, model mismatches, and nonlinear interactions between control subsystems [1]. These factors degrade system performance, especially in complex combat scenarios. To address these limitations, the integrated guidance and control (IGC) framework has been proposed, in which both subsystems are synthesized simultaneously within a unified control system [1], [2].

[*] Corresponding author, email: toandh@lqdtu.edu.vn
DOI: 10.56651/lqdtu.jst.v21.n1.1056

Various methods have been proposed for IGC systems, with backstepping being widely adopted due to its suitability for strict-feedback systems and its Lyapunov-based stability proof [3]–[5]. To improve disturbance rejection and uncertainty handling, backstepping methods integrated with extended state observers (ESO) have been widely used in AV control systems [6]–[9]. Recent studies have explored combining backstepping with sliding mode control (SMC) to improve responsiveness and robustness [10]–[14]. More recently, finite-time backstepping (FTB) control methods and finite-time disturbance observers (FTDO) have attracted considerable attention due to their ability to ensure that errors converge to zero within a finite time, rather than only asymptotically as in traditional methods [15]–[18]. Some recent studies have also initially combined the FTB and FTDO methods in AV control under specific system structure conditions or physical constraints [15], [16]. However, globally, studies that simultaneously combine both FTB and FTDO within IGC systems-while accounting for full model uncertainties, disturbances, and target maneuvers-remain scarce. In Vietnam, several studies have applied backstepping and SMC methods to IGC systems; however, no research has yet developed an FTB approach combined with FTDO for this class of systems. Most existing studies have so far employed either FTB or FTDO individually, without implementing them in a unified manner for real-time integrated control under strong disturbances and uncertainties as in AV systems.

This article addresses the gap by proposing a novel integrated control architecture that combines the FTB method with the FTDO observer to overcome the aforementioned limitations, enabling effective AV control under conditions of strong disturbances and uncertainties. The article is structured as follows: Section 2 presents the AV IGC dynamic model; Section 3 details the FTB controller and FTDO observer design; Section 4 presents simulation results and performance analysis; Section 5 provides conclusions and future research directions.

2. Problem formulation

2.1. Integrated guidance and control system model

Figure 1 [8] illustrates the motion of the AV and the target in the vertical plane, where OXY denotes the inertial Cartesian coordinate system, and M (AV) and T (target) respectively represent the quantities of the AV and the target. Here x_m, y_m and x_T, y_T are current position coordinates of the AV and target; V_M, θ_M, a_M are velocity,

flight path angle, and normal acceleration of the AV; V_T, θ_T, a_T are velocity, flight path angle, and normal acceleration of the target, respectively; R is relative distance between the AV and the target; q is line-of-sight (LOS) angle; $O_m x_b$ is AV body axis; ϑ is pitch angle of the AV.

The AV's kinematics in the vertical plane are shown in Fig. 2 [8], with the following notations: α is angle of attack; M_g, X_{aero}, Y_{aero} are gravitational force, aerodynamic drag and lift forces.

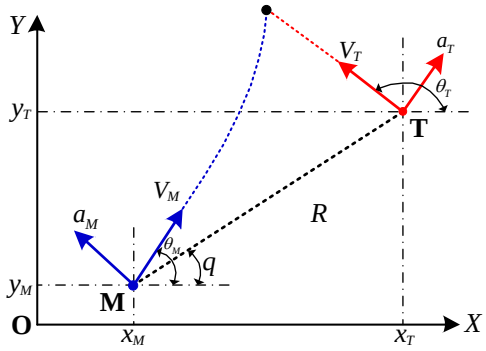

Fig. 1. Relative motion of AV and target in the vertical plane.

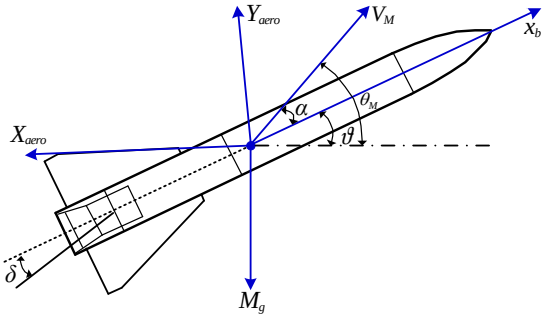

Fig. 2. AV dynamics in the vertical plane.

From Figs. 1, 2, the kinematic equations of the AV-target engagement are given as follows [8]:

$$\begin{aligned}
&\dot{R} = V_T \cos\left(q-\theta_T\right) - V_m \cos\left(q-\theta_M\right) \\
&R\dot{q} = -V_T \sin\left(q-\theta_T\right) + V_m \sin\left(q-\theta_M\right) \\
&\dot{\theta}_T = \frac{a_T}{V_T} \;,\; \dot{\theta}_M = \frac{a_M}{V_M}
\end{aligned} \tag{1}$$

To rewrite the original engagement dynamics into a strict-feedback form suitable for backstepping control, assuming that $\dot{V}_T = \dot{V}_M = 0$, we transform system (1) as follows:

$$\ddot{q} = -\frac{2\dot{R}}{R}\dot{q} + \frac{a_T \cos\left(q-\theta_T\right)}{R} - \frac{a_M \cos\left(q-\theta_M\right)}{R} \tag{2}$$

The dynamic equation of the AV in pitch motion is described as [8]:

$$\begin{aligned}
&\dot{\alpha} = \frac{1}{mV_M}\left(-L + mg\cos\theta_M\right) + \omega_z \\
&J_z\dot{\omega}_z = M_0 + M_z^{\delta_z}\delta_z \;;\; \dot{\vartheta} = \omega_z \;;\; \alpha = \vartheta - \theta_M
\end{aligned} \tag{3}$$

where m is the AV mass, ω_z is the AV pitch angular velocity, δ_z is the fin deflection angle about the z-axis, J_z is the moment of inertia of the device with respect to the z-axis, and ϑ is the pitch angle. $M_z^{\delta_z}$ is the control moment component that generates angular acceleration, M_0 represents the effects of other factors on the angular acceleration, and L is the lift force, which is commonly approximated under the small-angle assumption for α, as follows [8]:

$$\begin{cases} M_0 = M_\alpha \alpha + M_{\omega_z}\omega_z = 57.3QSlm_z^\alpha \alpha + \dfrac{QSl^2 m_z^{\omega_z}}{V_M}\omega_z \\ L = 57.3QS(c_y^\alpha \alpha + c_y^{\delta_z}\delta_z)\ ;\ a_m = -g\cos\theta_m + \dfrac{57.3QSc_y^\alpha \alpha}{m} \end{cases}$$

Q is the dynamic pressure, S is the reference area of the AV, c_y^α, $c_y^{\delta_z}$ are the lift force derivatives with respect to α, δ_z. The quantities $m_z^\alpha, m_z^{\omega_z}, m_z^{\delta_z}$ are the pitch channel moment derivatives with respect to α, ω_z, δ_z, respectively.

To obtain a simplified and tractable pitch-dynamics model, and to explicitly isolate the control effectiveness, Eq. (3) is rewritten as follows:

$$\dot{\alpha} = -\frac{Y^\alpha}{mV_M}\alpha + \frac{g\cos\theta_M}{V_M} + \omega_z = -\frac{57.3QSc_y^\alpha}{mV_M}\alpha + \frac{g\cos\theta_M}{V_M} + \omega_z \tag{4}$$

Let the state variables be defined as $x_1 = \dot{q},\ x_2 = \alpha,\ x_3 = \omega_z$ and control input as $u = \delta_z$. Considering system disturbances and uncertainties (referred to as lumped disturbances), combining Eqs. (2)-(4), we formulate the integrated guidance and control (IGC) system as:

$$\begin{cases} \dot{x}_1 = f_1(x_1) + g_1(x_1)x_2 + d_1 \\ \dot{x}_2 = f_2(x_2) + g_2(x_2)x_3 + d_2 \\ \dot{x}_3 = f_3(x_3) + g_3(x_3)u + d_3 \end{cases} \tag{5}$$

$$\begin{cases} f_1(x_1) = -\dfrac{2\dot{R}}{R}\dot{q} + \dfrac{g\cos(q-\theta_M)}{R}\cos\theta_M \\ f_2(x_2) = -\dfrac{57.3QSc_y^\alpha}{mV_M}\alpha + \dfrac{g\cos\theta_M}{V_M} \\ f_3(x_3) = \dfrac{57.3QSlm_z^\alpha}{J_z}\alpha + \dfrac{QSl^2 m_z^\omega}{J_z V_M}\omega_z \end{cases}, \begin{cases} g_1(x_1) = -\dfrac{57.3QSc_y^\alpha}{mR}\cos(q-\theta_M) \\ g_2(x_2) = 1 \\ g_3(x_3) = \dfrac{57.3QSlm_z^{\delta_z}}{J_z} \end{cases}, \begin{cases} d_1 = \dfrac{a_T\cos(q-\theta_T)}{R} \\ d_2 = d_2(c_y^\alpha, \Delta_2) \\ d_3 = d_3(m_z^\alpha, m_z^{\omega_z}, \Delta_3) \end{cases} \tag{6}$$

For notational simplicity, the functions $f_i(x_i)$, $g_i(x_i)$ and the associated engagement quantities are written without an explicit time argument. The functions in (5), (6) follow directly from the aerodynamic and kinematic relations. Since *q*, *R*, and a_T are measurable, physically bounded, and vary slowly during interception, the resulting $f_i(x_i)$, $g_i(x_i)$ are smooth and bounded time-varying functions that satisfy the uniformly ultimately bounded (UUB) condition required for finite-time backstepping and FTDO design [19]. Moreover, because all state variables x_1, x_2, x_3 and engagement parameters are measurable, the deterministic components of $f_i(x_i)$, $g_i(x_i)$ can be fully compensated in the control design, consistent with the modeling assumptions in [8], [10], [12], [13].

2.2. Integrated guidance and control design objective

In equation (5), the first equation represents the guidance law, where the disturbance d_1 mainly originates from the maneuvering of the target, characterized by the target's normal acceleration α_T and flight path angle θ_T. The second and third equations are the control laws: the second relates to the angle of attack, with disturbance d_2 mainly due to variations in the aerodynamic lift coefficient derivative c_y^{α}. The third equations to the pitch rate, with disturbance d_3 dependent on derivatives of the aerodynamic moment coefficient m_z^{α}, $m_z^{\omega_z}$ and $m_z^{\delta_z}$ center of gravity shifts, and air density fluctuations. The Δ_2 and Δ_3 represent external disturbances, including unmodeled aerodynamic effects, parameter variations, and other uncertainties. These factors are lumped together with modeling errors and jointly act on the control channels, forming the total lumped disturbances.

Assumption 1. (a) For the disturbances in system (5), there exist positive constants $\bar{d}_1, \bar{d}_2, \bar{d}_3$ such that d_1, d_2, d_3 and their first derivatives are bounded $\left|\frac{d^r d_i}{dt^r}\right| \le \bar{d}_i.\ (i = 1,...,3,\ r = 0,1)$.

(b) Due to the physical limits of the actuator ($\underline{\delta}_z, \bar{\delta}_z$) the deflection angle δ_z is constrained within a bounded set.

Assumption 2. During the entire guidance process, the relative distance: $\dot{R}(t) < 0;\ 0 < R(t) < R(0),\ t > 0$. Interception occurs when $R(t) \neq 0$ provided that the Line-of-Sight (LOS) rate $R^0 \in [R_{\min}, R_{\max}] = [0.01,\ 0.8]$m.

As is well known, direct interception can be achieved by driving the LOS rate to zero, i.e., implementing $\dot{q} \to 0$ in the guidance law design. In this article, the goal is to design an integrated guidance and control system under the presence of disturbances and control input constraints. Based on the above analysis and assumptions, the control objective is stated as follows: Design an IGC law for the AV system described by model (6), under the conditions in Assumption 1, such that:

$$\sup_{t\in[t_0,\infty]} \left|\dot{q}-0\right| \le \bar{q}, \quad \sup_{t\in[t_0,\infty]} \left|\alpha-\alpha_d\right| \le \bar{\alpha}, \quad \sup_{t\in[t_0,\infty]} \left|\omega_z-\omega_{zd}\right| \le \bar{\omega}_z$$

there exist positive constants $\bar{q}$, $\bar{\alpha}$, $\bar{\omega}_z$ representing the acceptable tracking error thresholds between the actual outputs x_i and the desired references x_{id}. Here, α_d denotes the commanded angle of attack generated by the guidance loop, and ω_{zd} denotes the commanded pitch rate generated by the control loop. The proposed IGC law must ensure that the control errors in subsystems x_2 and x_3 converge to a residual set containing the origin in finite time.

Assumption 3. $\left|g_i(x_i)\right| \ge g_{i,\min} > 0,\ \forall x_i,\ i=1,2,3.$

This assumption ensures that the control effectiveness does not vanish, allowing the terms involving $1/g_i(x_i)$ in the backstepping design to remain well-defined and preserving the strict-feedback structure required for finite-time stability.

3. IGC controller design based on finite-time backstepping combined with finite-time disturbance observer

3.1. Design of the finite-time disturbance observer

To improve the estimation and disturbance compensation performance while ensuring finite-time stability for the IGC system, this article proposes applying a finite-time disturbance observer (FTDO). Unlike traditional methods such as the Extended state observer, FTDO ensures fast convergence within a finite time, meeting stringent requirements for speed and stability in finite-time backstepping control.

Consider the following nonlinear system with additive disturbances (in a reduced form without the explicit time argument):

$$\dot{x} = f(x,u) + d \tag{7}$$

where $x \in \mathbb{R}^3$ is the state vector, $u \in \mathbb{R}$ is the control input, and $f(x,u)$ is a known smooth nonlinear function describing the nominal system dynamics. The term d denotes

a lumped disturbance, which includes external perturbations and modeling uncertainties, and is assumed to be differentiable up to order *l*, with its *l-th* derivative satisfying a Lipschitz condition with constant *L*.

The FTDO is designed to estimate d in finite time using the measured state x. To illustrate the design procedure, we first consider a first-order FTDO structure as presented in [20]:

$$\begin{aligned} \dot{z}_d &= -\lambda_d L \,\mathrm{sign}\left(z_d - x\right) + f\left(x,u\right) \\ \hat{d} &= \dot{z}_d - f\left(x,u\right) \end{aligned} \tag{8}$$

where $\hat{d}$ is the estimated disturbance and z_d is the internal state of the observer. The parameter λ_d is a tunable gain that determines the convergence speed of the FTDO. The parameter L represents the Lipschitz constant that bounds the derivative of the disturbance. This bound is required by the finite-time stability analysis to ensure that the disturbance does not vary too rapidly. Because λ_d and L play fundamentally different roles – one being a tunable gain and the other a disturbance-related bound – they cannot be merged into a single parameter.

Based on the system model (5) and the observer form (8), and under Assumption 1, the proposed FTDO for the guidance loop of the IGC system is constructed as follows [20]:

$$\begin{aligned} \dot{z}_{d1} &= -\lambda_{d1} L_1 \,\mathrm{sign}\left(z_{d1} - x_1\right) + f_1\left(x_1\right) + g_1\left(x_1\right) x_2 \\ \hat{d}_1 &= \dot{z}_{d1} - f_1\left(x_1\right) - g_1\left(x_1\right) x_2 \end{aligned} \tag{9}$$

Similarly, under Assumption 1, FTDOs for the control loop are proposed as follows:

$$\begin{aligned} \dot{z}_{d2} &= -\lambda_{d2} L_2 \,\mathrm{sign}\left(z_{d2} - x_2\right) + f_2(x_2) + g_2(x_2) x_3 \\ \hat{d}_2 &= \dot{z}_{d2} - f_2(x_2) - g_2(x_2) x_3 \end{aligned} \tag{10}$$

$$\begin{aligned} \dot{z}_{d3} &= -\lambda_{d3} L_3 \,\mathrm{sign}\left(z_{d3} - x_3\right) + f_3(x_3) + g_3(x_3) u \\ \hat{d}_3 &= \dot{z}_{d3} - f_3(x_3) - g_3(x_3) u \end{aligned} \tag{11}$$

Here, for each $i = 1 \div 3$, $\hat{d}_i$ is the estimated disturbance d_i, z_{di} is the internal state of the *i-th* observer, λ_{di} is a gain for convergence speed of the *i-th* observer; whereas L_i scales the bound of the disturbance derivative and the growth of the nominal dynamics.

In the FTDO structure (9)–(11), the nonlinear feedback term uses the sign function sign(*e*) to ensure finite-time convergence of observation errors. This is

characteristic of finite-time observers, where the Lyapunov derivative can be made to decrease linearly or nonlinearly, ensuring zero error in finite time. However, due to the discontinuous nature of the sign(·) function, control signals may experience high-frequency oscillations (chattering) in numerical simulations or practical implementations. This can impact system stability, especially with actuators having rate limits or bandwidth constraints. To mitigate this issue, the sign function sign(e) is proposed to be replaced with a continuous saturation function (12):

$$\text{sat}(e) = \begin{cases} \text{sign}(e), & |e| > \delta_e \\ \dfrac{e}{\delta}, & |e| \le \delta_e \end{cases} \tag{12}$$

Applying Eq. (12), the modified FTDO equations become:

$$\begin{aligned} \dot{z}_{di} &= -\lambda_{di} L_i \,\text{sat}\left(z_{di} - x_i\right) + f_i\left(x_i\right) + g_i\left(x_i\right) x_{i+1} \\ \widehat{d}_i &= \dot{z}_{di} - f_i\left(x_i\right) - g_i\left(x_i\right) x_{i+1} \end{aligned} \tag{13}$$

Here, δ_e is the threshold for the transition region of the saturation function. This improved FTDO structure is applied in Section 5 and demonstrates significant effectiveness in terms of stability and estimation capability, even under strong or rapidly varying disturbances.

3.2. Design of the finite-time backstepping controller

The control design proceeds as follows:

Step 1: Virtual control law design for $\dot{q}$

Define the error: $e_1 = x_1 - x_{1d}$; $x_{1d} = 0$ (14)

Choose a Lyapunov function of the form: $V_1 = \dfrac{1}{2} e_1^2$

Under Assumption 2, the nominal functions $f_i(x_i)$, $g_i(x_i)$ are smooth and locally Lipschitz, guaranteeing the existence of $\dot{V}$ and enabling the Lyapunov-based finite-time backstepping design.

Compute $\dot{V}_1$ and choose the virtual control $x_{2\text{d}}$ such that $\dot{V}_1 \le 0$, ensuring finite-time stability. Using the disturbance decomposition $d_1 = \widehat{d}_1 + \tilde{d}_1$, the actual and desired dynamics of the control error e_1 are defined as follows [15]:

$$\begin{aligned} \dot{e}_1 &= \dot{x}_1 - \dot{x}_{1d} = f_1(x_1) + g_1(x_1) x_2 + \widehat{d}_1 + \tilde{d}_1 - \dot{x}_{1d}) \\ &= -k_{11} |e_1|^{\mu_1} \,\text{sign}(e_1) - k_{12} |e_1|^{\nu_1} \,\text{sign}(e_1) - k_{13} e_1 \end{aligned} \tag{15}$$

where k_{11}, k_{12}, $k_{13} > 0$ are positive constants and $0 < \mu_1 < 1 < \nu_1$. Neglecting estimation error $\tilde{d}_1$, and solving for x_2, we obtain:

$$x_{2d} = \frac{1}{g_1(x_1)}(-f_1(x_1) - \hat{d}_1 + \dot{x}_{1d} + \dot{e}_1) \tag{16}$$

Substituting $\dot{e}_1$ from (15), we obtain:

$$x_{2d} = \frac{1}{g_1(x_1)}(-f_1(x_1) - \hat{d}_1 + \dot{x}_{1d} - k_{11}|e_1|^{\mu_1}\,\text{sign}(e_1) - k_{12}|e_1|^{\nu_1}\,\text{sign}(e_1) - k_{13}e_1) \tag{17}$$

Taking the time derivative of V_1 along the system trajectories yields

$$\dot{V}_1 = e_1\dot{e}_1 = -k_{11}|e_1|^{\mu_1+1} - k_{12}|e_1|^{\nu_1+1} - k_{13}e_1^2$$

Due to $\mu_1 + 1 < 2 < \nu_1 + 1$ we get $\dot{V}_1 \le -c_1 V_1^{\upsilon_1}$ with $0 < \upsilon_1 < \frac{\mu+1}{2} < 1$

From the finite-time Lyapunov theory [21], there exists $T_1 < \infty$ such that: $V_1(t) = 0 \Rightarrow e_1(t) = 0,\ \forall t \ge T_1$. Thus, the first-layer tracking error e_1 converges to zero in finite time.

Step 2: Design of the virtual control law for α

Define error: $e_2 = x_2 - x_{2d}$ (18)

Choose an extended Lyapunov function: $V_2 = V_1 + \frac{1}{2}e_2^2 = \frac{1}{2}e_1^2 + \frac{1}{2}e_2^2$

Compute $\dot{V}_2$ and choose the virtual control x_{3d} such that $\dot{V}_2 \le 0$, ensuring finite-time stability. With the disturbance decomposition $d_2 = \hat{d}_2 + \tilde{d}_2$, the actual and desired dynamics of the control error e_2 are defined as follows [15]:

$$\begin{aligned}\dot{e}_2 &= f_2(x_2) + g_2(x_2)x_3 + \hat{d}_2 + \tilde{d}_2 - \dot{x}_{2d} \\ &= -k_{21}|e_2|^{\mu_2}\,\text{sign}(e_2) - k_{22}|e_2|^{\nu_2}\,\text{sign}(e_2) - k_{23}e_2\end{aligned} \tag{19}$$

with positive constants k_{21}, k_{22}, $k_{23} > 0$ and $0 < \mu_2 < 1 < \nu_2$.

Neglecting estimation error $\tilde{d}_2$, we obtain the virtual control:

$$x_{3d} = \frac{1}{g_2(x_2)}(-f_2(x_2) - \hat{d}_2 + \dot{x}_{2d} - k_{21}|e_2|^{\mu_2}\,\text{sign}(e_2) - k_{22}|e_2|^{\nu_2}\,\text{sign}(e_2) - k_{23}e_2) \tag{20}$$

Taking the time derivative of V_2 along the system trajectories yields

$$\dot{V}_2 = e_1\dot{e}_1 + e_2\dot{e}_2 = -k_{11}|e_1|^{\mu_1+1} - k_{12}|e_1|^{\nu_1+1} - k_{13}e_1^2 - k_{21}|e_2|^{\mu_2+1} - k_{22}|e_2|^{\nu_2+1} - k_{23}e_2^2$$

Due to $\mu_2 + 1 < 2 < \nu_2 + 1$, $\dot{V}_2 \le -c_2 V_2^{\upsilon_2}$ with $\upsilon_2 = \frac{\min(\mu_1+1, \nu_1+1, \mu_2+1, \nu_2+1, 2)}{2} < 1$.

There exists $T_2 < \infty$ such that: $V_2(t) = 0 \Rightarrow e_1(t), e_2(t) \to 0,\ \forall t \ge T_2$.

Therefore, the first two layers of the control system achieve finite-time stability, with both tracking errors $e_1(t)$, $e_2(t)$ converging to zero in finite time.

At each recursive step of the finite-time backstepping design, the virtual controls $x_{2d}(e_1)$ and $x_{3d}(e_1, e_2)$ are chosen so that the intermediate errors e_1 and e_2 satisfy a finite-time Lyapunov condition. Considering the estimation errors $\tilde{d}_1$ and $\tilde{d}_2$, this ensures that both errors converge to vinicity of the origin in finite time, thereby verifying the required tracking behavior at each backstepping layer.

Step 3: Actual control law design for *u*

The objective is to design the actual control signal *u* such that the entire system achieves global finite-time stability.

Define the third-layer control error: $e_3 = x_3 - x_{3d}$ (21)

Choose the total Lyapunov function: $V_3 = V_2 + \frac{1}{2}e_3^2 = \frac{1}{2}e_1^2 + \frac{1}{2}e_2^2 + \frac{1}{2}e_3^2$.

Compute $\dot{V}_3$ and choose the virtual control u such that $\dot{V}_3 \le 0$, ensuring finite-time stability. With the disturbance decomposition $d_3 = \hat{d}_3 + \tilde{d}_3$, the desired dynamics of the virtual control are defined as follows [15]:

$$\begin{aligned}\dot{e}_3 &= f_3(x_3) + g_3(x_3)u + \hat{d}_3 + \tilde{d}_3 - \dot{x}_{3d} \\ &= -k_{31}|e_3|^{\mu_3}\,\mathrm{sign}(e_3) - k_{32}|e_3|^{\nu_3}\,\mathrm{sign}(e_3) - k_{33}e_3\end{aligned} \quad (22)$$

with positive constants k_{31}, k_{32}, $k_{33} > 0$ and $0 < \mu_3 < 1 < \nu_3$. Neglecting estimation error $\tilde{d}_3$, from equation $\dot{e}_3 = \dot{x}_3 - \dot{x}_{3d}$ and solving for *u*, we obtain:

$$u = \frac{1}{g_3(x_3)}(-f_3(x_3) - \hat{d}_3 + \dot{x}_{3d} - k_{31}|e_3|^{\mu_3}\,\mathrm{sign}(e_3) - k_{32}|e_3|^{\nu_3}\,\mathrm{sign}(e_3) - k_{33}e_{33}) \quad (23)$$

Under Assumption 1(b), the control input δ_z is bounded within the actuator limits, ensuring feasibility and preventing saturation.

Taking the time derivative of V_3 along the system trajectories yields

$$\dot{V}_3 = \dot{V}_2 + e_3\dot{e}_3 = -k_{11}|e_1|^{\mu_1+1} - k_{12}|e_1|^{\nu_1+1} - k_{13}e_1^2 - k_{21}|e_2|^{\mu_2+1} - k_{22}|e_2|^{\nu_2+1} - k_{23}e_2^2 - k_{31}|e_3|^{\mu_3+1} - k_{32}|e_3|^{\nu_3+1} - k_{33}e_3^2$$

Since $\mu_3+1<2<\nu_3+1$, it follows that $\dot{V}_3 \le -c_3V_3^{\upsilon 3}$, with:

$\upsilon_3 = \dfrac{\min(\mu_1+1, \nu_1+1, \mu_2+1, \nu_2+1, \mu_3+1, \nu_3+1, 2)}{2} < 1$, there exists a finite time T_3 such that $V_3(t) = 0$ for all $t \ge T_3$. Consequently, the tracking errors satisfy $e_1(t), e_2(t), e_3(t) \to 0$ as $t \to T_3$, or equivalently $x_i(t) \to x_{id}(t)$ for $i = 1 \div 3$.

Combining the three steps above, the overall error vector (e_1, e_2, e_3) is finite-time stable and converges to zero. Thus, the errors of all system states converge to zero in finite time, and the control system using the finite-time backstepping technique with the actual control *u* is designed to achieve global finite-time stability. Note that the estimation error of the FTDO appears in the controller as a bounded residual disturbance. During the transient phase, this error does not compromise stability, since the finite-time backstepping controller is ISS (Input-to-State Stability) with respect to such perturbations. After the FTDO converges in finite time, the residual error vanishes and the closed-loop IGC system satisfies the finite-time Lyapunov conditions, guaranteeing overall finite-time stability.

Remark 1. Since the FTDO guarantees finite-time convergence of the estimation error within a settling time T_d, disturbance compensation becomes exact after T_d. At this stage, the finite-time backstepping controller operates under perfect disturbance cancellation and fully satisfies the finite-time Lyapunov conditions. According to the finite-time cascade stability theorem [22], the combination of the FTDO and the FTB controller preserves finite-time stability of the overall IGC system, ensuring that the tracking errors converge to zero in finite time.

In both simulation and practical implementation, the sign(*e*) functions in the control law may cause chattering. To address this issue, the sign(*e*) functions are replaced by tanh(*e*) functions with slope adjustment coefficients $l_i > 0$ to smooth the control signal in the vicinity of the equilibrium point while maintaining fast convergence characteristics. The resulting expressions for the virtual control and the actual control *u* are then given as follows:

$$x_{2d} = \frac{1}{g_1(x_1)}(-f_1(x_1) - \hat{d}_1 + \dot{x}_{1d} - k_{11}|e_1|^{\mu_1}\tanh(l_1e_1) - k_{12}|e_1|^{\nu_1}\tanh(l_1e_1) - k_{13}e_1) \quad (24)$$

$$x_{3d} = \frac{1}{g_2(x_2)}(-f_2(x_2) - \hat{d}_2 + \dot{x}_{2d} - k_{21}|e_2|^{\mu_2}\tanh(l_2e_2) - k_{22}|e_2|^{\nu_2}\tanh(l_1e_2) - k_{23}e_2) \quad (25)$$

$$u = \frac{1}{g_3(x_3)}(-f_3(x_3) - \hat{d}_3 + \dot{x}_{3d} - k_{31}|e_3|^{\mu_3}\tanh(l_3e_3) - k_{32}|e_3|^{\nu_3}\tanh(l_3e_3) - k_{33}e_{33}) \quad (26)$$

4. Simulation and discussion

4.1. Simulation input parameters

To verify the effectiveness of the proposed control method, numerical simulations are conducted to evaluate the responsiveness and accuracy of the FTB control structure and the FTDO observer for the designed IGC system. The simulation of the finite-time backstepping controller combined with a finite-time disturbance observer (denoted FTB-FTDO) is compared with that of a backstepping controller combined with a reduced-order extended state observer (denoted Back-RESO) [8]. The controller and observer parameters in the simulations are selected to be dynamically equivalent to ensure an objective comparison and evaluation. In the simulations, the AV and target are assumed to travel at constant speeds, while the target is capable of maneuvering with a time-varying normal acceleration. The parameters of the homing AV used in this study are assumed as follows [8]: Initial relative distance between AV and target $R_0 = 10$ km; Initial Line-of-Sight (LOS) angle $q_0 = 30°$; Constant AV speed $V_M = 500$ m/s. Initial AV flight path angle $\alpha_0(0) = 0$, $\delta_z(0) = 0$, $\theta_M(0) = 45°$. Constant target speed $V_T = 250$ m/s. Initial target flight path angle $\theta_T(0) = 120°$. The AV model parameters are as follows:

$$\frac{57.3QSc_y^{\alpha}}{mV_M} = 0.3487;\ \frac{57.3QSlm_z^{\alpha}}{J_z} = -17.801;\ \frac{QSl^2m_z^{w_z}}{J_zV_M} = -0.2741;\ \frac{57.3QSlm_z^{\delta_z}}{J_z} = -31.267$$

The actuator (rudder deflection angle) is constrained by the control limit $|\delta_z| \le 20°$ [7]. The design coefficients for the conventional backstepping controller are: $k_1 = 0.4$, $k_2 = 4.0$, $k_3 = 12$. The design coefficients for the proposed FTB controller are $k_{11} = 0.5$, $k_{12} = 0.5$, $k_{13} = 0.4$, $k_{21} = 0.5$, $k_{22} = 0.5$, $k_{23} = 4.0$, $k_{31} = 0.5$, $k_{32} = 0.5$, $k_{33} = 12$.

The design coefficients for the RESO observer are: $\beta_1 = 5$, $\beta_2 = 10$, $\beta_3 = 20$. The design coefficients for the proposed FTDO observer are:

$\lambda_{d1} = 5,\ \lambda_{d2} = 10,\ \lambda_{d3} = 20,\ L_1 = 0.5,\ L_2 = 0.3,\ L_3 = 0.5$

Simulations are conducted under two scenarios:

Case 1: The target is non-maneuvering, the AV's normal acceleration is zero so $d_1 = 0$, the AV's aerodynamic coefficients are assumed to be constant throughout the engagement; the external disturbances applied are $\Delta_2 = 0.5\sin(t)$ and $\Delta_3 = 0.2\sin t.$

Case 2: Suppose that the coefficients of aerodynamics forces and moments are all reduced by -25% of their respective nominal values; the target maneuvers with a normal acceleration of $a_T = 60\sin(0.5t)(\text{m/s}^2)$. Additionally, external disturbances are added to the control loop dynamicsdisturbance: $\Delta_2 = 0.5\sin(t)$ and is additionally affected by a signal $\Delta_{2a} = 0.25$ at time $t_1 = 10\text{s}$; $\Delta_3 = 0.35\sin(t)$ is additionally affected by a signal $\Delta_{3a} = 0.01t$ at time $t_2 = 10\text{s}$.

4.2. Simulation results and analysis

a) The simulation results for Case 1 are shown in Figs. 3-6.

The simulation results of the guidance loop in Case 1 include the AV and target trajectories (Fig. 3); the distance between the AV and the target; the LOS angular rate; and the AV acceleration, as presented in Fig. 4. The simulation results of the control loop states in Case 1 are presented in Fig. 5. The disturbance estimation results using the Back-RESO and FTB-FTDO controllers in Case 1 are shown in Fig. 6.

Figure 3 illustrates the AV-target interception trajectories obtained with the two controllers. Both closely follow the target path and achieve a successful intercept after a certain period. However, the trajectory controlled by the FTB-FTDO scheme responds faster, which reflects its finite-time convergence property. The target interception times are $T_{1.Back-RESO} = 23.24$ s, $T_{1.FTB-FTDO} = 23.20$ s; and the distances at interception are $R_{1.Back-RESO} \le 0.35$ m, $R_{1.FTB-FTDO} \le 0.31$ m, showing that FTB-FTDO shortens interception time and improves accuracy. Figure 4 presents the guidance loop simulation results for Case 1 with both controllers. Since the target is non-maneuvering, the outcomes are generally similar and follow the expected system behavior. Nevertheless, FTB-FTDO exhibits clear advantages in the initial and final phases. Specifically, the range curve R almost overlaps in both cases and converges to zero, indicating precise guidance. However, the LOS rate and AV acceleration with FTB-FTDO show less oscillation and converge to the desired values more quickly. Figure 5 shows the control

loop state variables in Case 1. The angle of attack α decreases gradually toward zero, while ω_z oscillates at the disturbance frequency with diminishing amplitude, contributing to system stability. The control signal u stabilizes quickly for both methods, but with FTB-FTDO the initial amplitude is smaller and the variation smoother, reducing actuator load. Figure 6 shows the disturbance and disturbance estimation errors results for the two observers, RESO and FTDO. Both achieve good estimation performance with small, stable errors for d_2, d_3. However, FTDO tracks disturbances more accurately, especially for oscillatory signals d_2, d_3, by reducing phase and amplitude errors. This demonstrates that FTDO's finite-time convergence property improves estimation speed and accuracy.

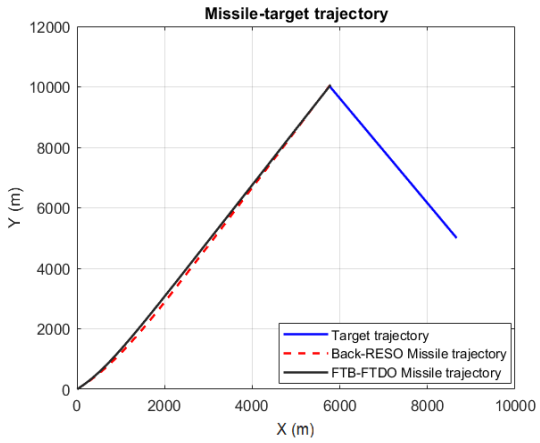

Fig. 3. Simulation results of the AV-target trajectory in Case 1.

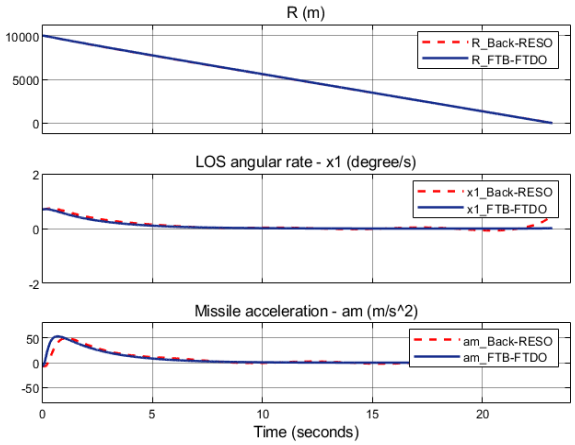

Fig. 4. Simulation results of the guidance loop in Case 1.

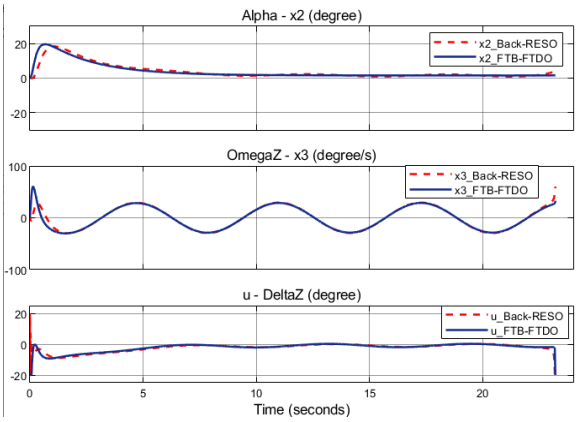

Fig. 5. Simulation results of the control loop states in Case 1.

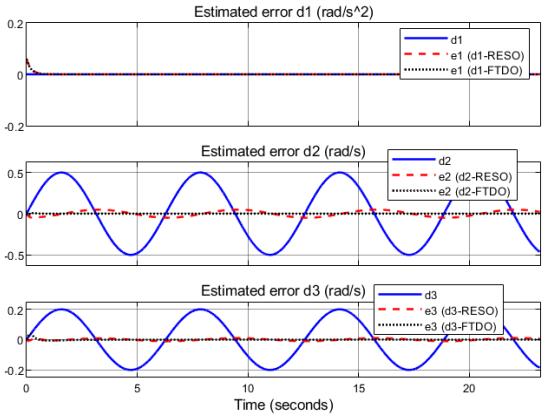

Fig. 6. Estimation error for disturbances with Back-RESO and FTB-FTDO in Case 1.

b) The simulation results for Case 2 are shown in Figs. 7-12.

The corresponding simulation results for Case 2 are shown in the following figures. Figure 7 illustrates the trajectories of the AV and target in Case 2 when using the two controllers: Back-RESO and FTB-FTDO. Both AV trajectories closely follow the target path, ensuring successful interception after a certain time. However, the differences between the two control methods become more pronounced compared to Case 1. Specifically, the AV trajectory under the FTB-FTDO controller is smoother, exhibits less oscillation, and tracks the target more closely throughout the guidance process. This reflects the fast and stable response capability of the FTB-FTDO controller to changes in the target's trajectory. At the interception moment, the time to intercept the target is $T_{2.Back-RESO} = 18.15\text{s}$, $T_{2.FTB-FTDO} = 17.84\text{s}$; and the AV-target distance at interception is $R_{2.Back-RESO} \le 0.51\text{m}$, $R_{2.FTB-FTDO} \le 0.39\text{m}$. These results demonstrate that the FTB-FTDO controller not only shortens interception time but also improves accuracy. This advantage stems from the finite-time convergence structure of the FTB-FTDO method, allowing the control system to respond quickly and adjust effectively to disturbances and maneuvering targets.

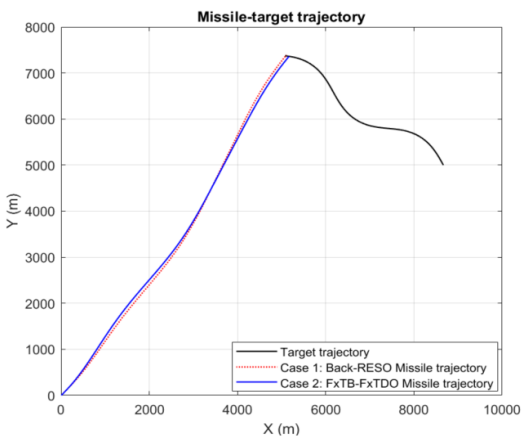

Fig. 7. Simulation results of the AV-target trajectory in Case 2.

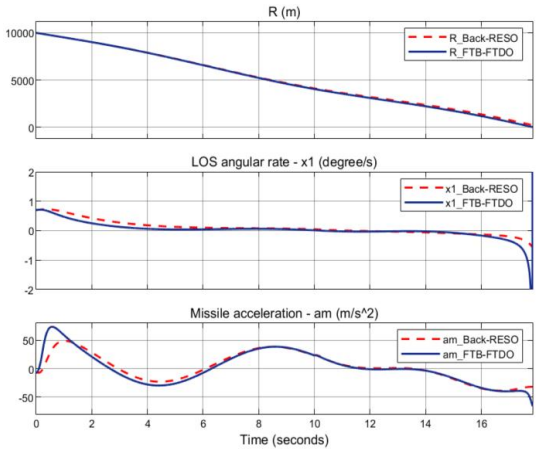

Fig. 8. Simulation results of the guidance loop in Case 2.

Figure 8 shows that the distance R steadily decreases toward zero in both cases, ensuring accurate guidance. However, the R curve for FTB-FTDO decreases faster near the end of the trajectory, reflecting its rapid response characteristic. The LOS angular rate when using FTB-FTDO oscillates less and converges more quickly to zero, contributing to better stabilization of the line-of-sight angle. Additionally, the AV acceleration controlled by FTB-FTDO is smoother and exhibits fewer fluctuations compared to

Back-RESO, reducing overshoot phenomena and enhancing accuracy while alleviating stress on the AV structure. Figure 9 presents the system states within the control loop using both controllers. The angle of attack α initially oscillates and then gradually decreases toward zero, indicating a stabilizing system trend. The angular velocity ω_z oscillates at frequencies corresponding to the disturbances, but the amplitude of these oscillations remains low. The control command δ_z reacts swiftly to compensate for disturbances, especially during significant fluctuations. Comparing the two controllers, the FTB-FTDO controller exhibits a faster response, smaller oscillation amplitudes, and better system stability than Back-RESO, particularly during transient phases and in the presence of disturbances.

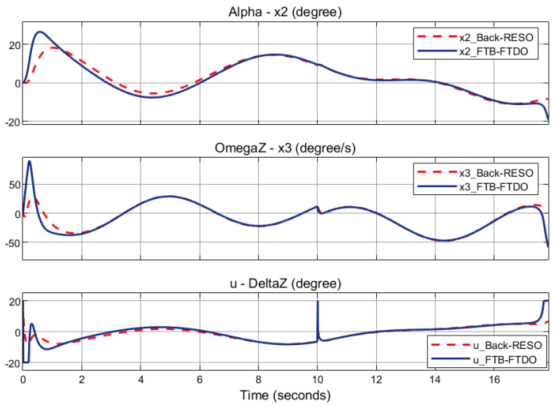

Fig. 9. Simulation results of the control loop states in Case 2.

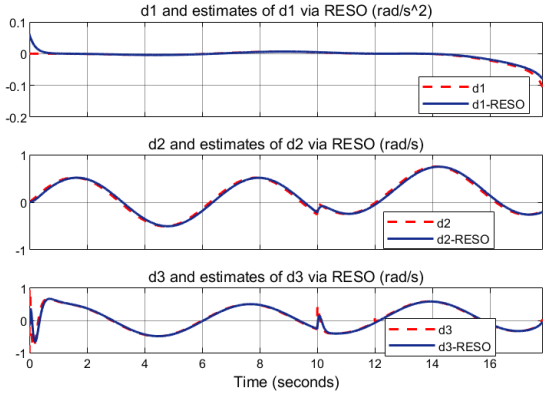

Fig. 10. Simulation estimates of disturbances via RESO in Case 2.

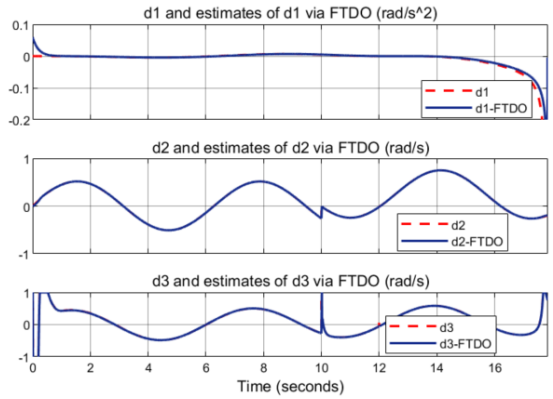

Fig. 11. Simulation estimates of disturbances via FTDO in Case 2.

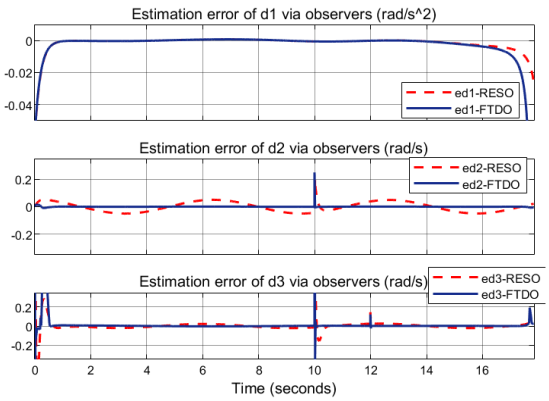

Fig. 12. Estimation errors of disturbances via the state observers in Case 2.

Figures 10-12 compare the disturbance-estimation performance of RESO and FTDO. Both observers are able to reconstruct the disturbances; however, clear differences appear, especially for the oscillatory components d_2 and d_3. As shown in the figures, RESO suffers from amplitude attenuation and noticeable phase lag, whereas FTDO generates estimates that almost overlap the true disturbance signals, accurately preserving both amplitude and phase. At $t = 10\,\mathrm{s}$, the lumped disturbances d_2 and d_3 undergo sudden changes (caused by the injected disturbances Δ_2 and Δ_3), leading to corresponding jumps in the estimation errors e_{d2} and e_{d3}. After these abrupt variations, both observers drive their estimation errors back toward zero. Quantitative analysis in Figs. 10-12 shows that FTDO recovers considerably faster. Using a 5%-of-peak error threshold for d_2 and d_3, the corresponding convergence times are:

Convergence time (T_c) for d_2: RESO: $T_{c2\text{-RESO}} = 0.13$ s; FTDO: $T_{c2\text{-FTDO}} = 0.012$ s.

Convergence time for d_3: RESO: $T_{c3\text{-RESO}} = 0.063$ s; FTDO: $T_{c3\text{-FTDO}} = 0.014$ s.

Similarly, the mean-square estimation errors (computed with respect to the nominal value 0) also highlight the advantage of FTDO:

MSE(e_{d2}-RESO) = 1.24×10^{-4} rad/s; MSE(e_{d2}-FTDO) = 5.06×10^{-6} rad/s.

MSE(e_{d3}-RESO) = 5.83×10^{-4} rad/s; MSE(e_{d3}-FTDO) = 1.63×10^{-4} rad/s.

These results quantitatively confirm that the finite-time nonlinear structure of FTDO enables substantially faster convergence, smaller residual errors, and more accurate tracking of fast-varying disturbances than the asymptotic behavior of RESO.

5. Conclusion

This work has developed an integrated guidance and control scheme that achieves finite-time stability in the presence of model uncertainties and external disturbances by combining a finite-time backstepping controller with a finite-time disturbance observer. The synergy between the two components allows the control law to rapidly compensate lumped disturbances and improves the robustness and responsiveness of the overall IGC system. Simulation results confirm that the proposed method reduces interception time, decreases tracking and terminal errors, and maintains reliable performance even under strong disturbances and highly maneuvering targets. These results demonstrate the practical effectiveness of finite-time disturbance estimation when incorporated into a finite-time control framework. Future research will focus on extending the approach to

higher-dimensional 3-DOF/6-DOF IGC models, accounting for cross-coupling aerodynamics, and integrating advanced state-estimation filters to further enhance robustness against sensor noise and parameter variations.

References

[1] P. K. Menon and E. J. Ohlmeyer, "Integrated design of agile missile guidance and autopilot systems", *Control Engineering Practice*, Vol. 9, Iss. 10, pp. 1095-1106, 2001. DOI: 10.1016/S0967-0661(01)00082-X

[2] M. Z. Hou, X. L. Liang, and G. R. Duan, "Adaptive block dynamic surface control for integrated missile guidance and autopilot", *Chinese Journal of Aeronautics*, Vol. 26, Iss. 3, pp. 741-750, 2013. DOI: 10.1016/j.cja.2013.04.035

[3] H. Yan, X. H. Wang, B. F. Yu, and H. B. Ji, "Adaptive integrated guidance and control based on backstepping and input-to-state stability", *Asian Journal of Control*, Vol. 16, No. 2, pp. 602-608, 2014. DOI: 10.1002/asjc.682

[4] S. H. Seyedipour, M. Fathi, and S. Shamaghdari, "Nonlinear integrated guidance and control based on adaptive backstepping scheme", *Aircraft Engineering and Aerospace Technology*, Vol. 89, No. 3, pp. 415-424, 2017. DOI: 10.1108/AEAT-12-2014-0209

[5] Pei Pei, Y. Ji, S. He, J. Wang, and D. Lin, "Integrated guidance and control using adaptive backstepping approach for maneuvering target interception", *IFAC-PapersOnLine*, Vol. 53, Iss. 2, pp. 9458-9464, 2020. DOI: 10.1016/j.ifacol.2020.12.2418

[6] J. Han, "From PID to active disturbance rejection control", *IEEE Transactions on Industrial Electronics*, Vol. 56, Iss. 3, pp. 900-906, 2009. DOI: 10.1109/TIE.2008.2011621

[7] Z. Zhu, D. Xu, J. Liu, and Y. Xia, "Missile guidance law based on extended state observer", *IEEE Transactions on Industrial Electronics*, Vol. 60, Iss. 12, pp. 5882-5891, 2013. DOI: 10.1109/TIE.2012.2232254

[8] S. Xingling and W. Honglun, "Back-stepping active disturbance rejection control design for integrated missile guidance and control system via ESO", *ISA Transactions*, Vol. 57, pp. 232-246, 2015. DOI: 10.1016/j.isatra.2015.02.013

[9] L. Wang, W. Zhang, D. Wang, K. Peng, and H. Yang, "Command filtered back-stepping missile integrated guidance and autopilot based on extended state observer", *Advances in Mechanical Engineering*, Vol. 9, Iss. 11, 2017. DOI: 10.1177/1687814017733251

[10] M. Ran, Q. Wang, H. Delong, and C. Dong, "Backstepping design of missile guidance and control based on adaptive fuzzy sliding mode control", *Chinese Journal of Aeronautics*, Vol. 27, Iss. 3, 2014. DOI: 10.1016/j.cja.2014.04.007

[11] Q. Wang, M. Ran, and C. Dong, "Robust partial integrated guidance and control for missiles via extended state observer", *ISA Transactions*, Vol. 65, pp. 27-36, 2016. DOI: 10.1016/j.isatra.2016.08.017

[12] J. Guo, Y. Xiong, and J. Zhou, "A new sliding mode control design for integrated missile guidance and control system", *Aerospace Science and Technology*, Vol. 78, pp. 671-682, 2018. DOI: 10.1016/j.ast.2018.03.042

[13] K. Niu, X. Chen, D. Yang, J. Li, and J. Yu, "A new sliding mode control algorithm of IGC system for intercepting great maneuvering target based on EDO", *Sensors*, Vol. 22, Art. No. 7618, 2022. DOI: 10.3390/s22197618

[14] N. M. Tú và N. V. Thuận, "Nghiên cứu tổng hợp luật điều khiển trượt cho thiết bị bay với hệ thống dẫn và điều khiển tích hợp", *Journal of Science and Technique*, Vol. 19, No. 02, tr. 49-64, 2024. DOI: 10.56651/lqdtu.jst.v19.n02.793

[15] N. Patel, C. K. Paul, I. N. Kar, and S. Mukherjee, "Finite time adaptive backstepping control approach for quadrotors", *IFAC-PapersOnLine*, Vol. 57, pp. 89-94, 2024. DOI: 10.1016/j.ifacol.2024.05.016

[16] Z. Chong, J. Guo, and X. Lu, "Finite-time integrated guidance and control system for hypersonic vehicles", *Transactions of the Institute of Measurement and Control*, Vol. 43, Iss. 4, pp. 767-776, 2021. DOI: 10.1177/0142331220941934

[17] E. Duraffourg, L. Burlion, and T. Ahmed-Ali, "Finite-time observer-based backstepping control of a flexible launch vehicle", *Journal of Vibration and Control*, Vol. 24, No. 8, pp. 1535-1550, 2017. DOI: 10.1177/1077546316664021

[18] M. H. Nguyen and K. K. Ahn, "A finite-time disturbance observer for tracking control of nonlinear systems subject to model uncertainties and disturbances", *Mathematics*, Vol. 12, Iss. 22, 2024. DOI: 10.3390/math12223512

[19] M. Moulay and W. Perruquetti, "Finite time stability conditions for non autonomous continuous systems", *International Journal of Control*, Vol. 81, Iss. 5, pp. 797-803, 2008. DOI: 10.1080/00207170701650303

[20] S. Li, J. Yang, W. H. Chen, and X. Chen, *Disturbance Observer-Based Control: Methods and Applications*, 1st edition, Boca Raton: CRC Press, 2014. DOI: 10.1201/b16570

[21] F. Zheng, Z. Li, Z. Jia, J. Li, and J. Yu, "Dynamic modeling and observer-based fixed-time backstepping control for a hypersonic morphing waverider", *Applied Sciences*, Vol. 14, Iss. 13, Art. No. 5924, 2024. DOI: 10.3390/app14135924

[22] S. P. Bhat and D. S. Bernstein, "Finite-time stability of continuous autonomous systems", *SIAM Journal on Control and Optimization*, Vol. 38, No. 3, pp. 751-766, 2000. DOI: 10.1137/S0363012997321358

THIẾT KẾ BỘ ĐIỀU KHIỂN THÍCH NGHI THỜI GIAN HỮU HẠN CHO CÁC HỆ THỐNG DẪN–ĐIỀU KHIỂN TÍCH HỢP SỬ DỤNG BỘ QUAN SÁT NHIỄU THỜI GIAN HỮU HẠN VÀ KỸ THUẬT BACKSTEPPING

Đinh Hồng Toàn[1], Trương Đăng Khoa[1], Mai Ngọc Anh[2],
Phạm Văn Nguyên[1], Trần Quý[1], Nguyễn Công Định[1]
[1]*Viện Kỹ thuật điều khiển, Trường Đại học Kỹ thuật Lê Quý Đôn*
[2]*Trung tâm Công nghệ, Trường Đại học Kỹ thuật Lê Quý Đôn*

Tóm tắt: Bài báo đề xuất một phương pháp tổng hợp điều khiển mới cho hệ thống dẫn và điều khiển tích hợp của thiết bị bay, dựa trên kỹ thuật backstepping thời gian hữu hạn (FTB) kết hợp với bộ quan sát nhiễu thời gian hữu hạn (FTDO). Khác với các phương pháp backstepping truyền thống vốn chỉ đảm bảo hội tụ tiệm cận, phương pháp này bảo đảm hội tụ trong thời gian hữu hạn và tăng cường đáng kể khả năng chống nhiễu. Bộ điều khiển được thiết kế theo cấu trúc strict-feedback, trong đó mỗi hệ con được ổn định bằng các luật điều khiển phi tuyến thỏa mãn điều kiện ổn định Lyapunov. Các bộ quan sát nhiễu thời gian hữu hạn riêng biệt được xây dựng cho từng phương trình trạng thái nhằm ước lượng chính xác nhiễu tổng hợp và nâng cao hiệu quả bù sai lệch. Kết quả mô phỏng cho thấy phương pháp đề xuất giúp rút ngắn thời gian quá độ, giảm sai số điều khiển và duy trì khả năng bám sát mục tiêu chính xác ngay cả trong điều kiện nhiễu mạnh.

Từ khóa: *Dẫn và điều khiển tích hợp (IGC); backstepping thời gian hữu hạn (FTB); bộ quan sát nhiễu thời gian hữu hạn (FTDO); mục tiêu cơ động; nhiễu tổng.*

Received: 13/08/2025; Revised: 02/12/2025; Accepted for publication: 27/01/2026

❑